Launching low energy surface plasmons in purple gold ($AuAl_2$)

Panupon Samaimongkol and Hans D. Robinson*

Dept. of Physics, Virginia Tech, Blacksburg, VA 24061, USA

ABSTRACT: We confirm that the unusual purple color of the intermetallic compound $AuAl_2$ is of a plasmonic origin by launching surface plasmons (SPs) in thin $AuAl_2$ films. We measure the SP dispersion relation and also use the films to measure the index of refraction of sucrose solutions using standard SP resonance sensing. We find that the SP energy in planar $AuAl_2$ is approximately 2.1 eV, about 0.4 eV lower than in gold, and the material is highly resistant to oxidation. This is close to what is expected from previously reported measurements of the dielectric function of $AuAl_2$. On this basis we predict that $AuAl_2$ nanoparticles will a have very strong, spectrally nearly uniform light absorbance about an order of magnitude greater than standard carbon black. Such particles may therefore find applications as obscurants or as an alternative to more complex light absorbing gold structures in areas such as photothermal therapy or solar steam generation, or in plasmonic catalysis.

KEYWORDS: purple gold, surface plasmons, thin films, nanoparticles, light absorber

This is a post-peer-review, pre-copyedit version of an article published in Gold Bulletin. The final authenticated version is available online at

http://dx.doi.org/10.1007/s13404-018-0250-3

*CORRESPONDING AUTHOR.

email: hansr@vt.edu. tel.: +1-540-231-8732 (H.D.R)

ORCID: 0000-0003-0115-053X (P. S.), 0000-0003-3928-105X (H.D.R)

Of the five intermetallic compounds between Au and Al [1], the most aluminum-rich is $AuAl_2$, or purple gold. As this name suggests, $AuAl_2$ is distinguished by an intense and unusual purple color, first described by W. C. Robert-Austen in 1891 [2]. As it meets the definition of 18 carat gold, its main use today is as a decorative element in gold jewelry [3-5]. In a negative sense, it is also important technologically, as it occurs in gold wirebonds onto aluminum contact pads in integrated circuits, where its presence signifies a contact of poor reliability, which has earned the compound the moniker "purple plague". For this reason, there is an extensive literature studying the formation of intermetallics at the interface between gold and aluminum [1,6-10].

It was originally assumed that $AuAl_2$ derives its color from an interband absorption [11,12] akin to how copper and gold achieve their colors, although several authors have argued that the 5d band in this compound lies too far below the Fermi level for this to be plausible [13-15]. A recent calculation of the of $AuAl_2$ dielectric function ε suggested that low energy bulk plasmons play a pivotal role in the origin of the purple color [16]. The existence of bulk plasmons in purple gold was also verified by the same authors through electron energy-loss spectroscopy.

Specifically, interband absorption manifests as a broad plateau in the imaginary part ε_I of the dielectric function of a metal, while plasmons are associated with a zero crossing of the real part ε_R of the dielectric function. In gold, ε_I has a plateau with an onset of about 2.5 eV, well within the visible spectrum, while ε_R has a zero crossing at about 6 eV [17], too high in energy to generate a surface plasmon at visible wavelengths, at least on low curvature surfaces. In $AuAl_2$ the situation is the reverse, with ε_I taking on large values starting at 4 eV (comparable to what is seen in silver), and ε_R undergoing a zero crossing at about 3.8 eV [18], which should be low enough to enable surface plasmons at visible wavelengths, even on a completely flat surface.

In this Letter, we confirm this by demonstrating that surface plasmons (SPs) can be launched into thin $AlAu_2$ films just as in pure gold films. We extract a dispersion relation for the surface plasmon in purple gold and compare it to theory. We show that although surface plasmons in $AuAl_2$ are quite lossy, they still lend themselves to surface plasmon resonance (SPR) sensing. Finally, we discuss potential applications of $AuAl_2$ [19-22], which would be particularly promising in purple gold nanoparticles, if these could be fabricated.

As was recently pointed out by Naik et al. [23], the search for novel plasmonic materials is essential to realizing many concepts as practical technologies. They proposed transition metal nitrides and transparent conducting oxides as alternatives to Ag and Au for plasmonic applications. However, these materials do not possess surface plasmon resonances in the low-energy half of the visible spectrum (1.6 eV – 2.4 eV), which is quite rare. Among metals, only $AuAl_2$ and its analogs, including $AuGa_2$, $AuIn_2$ [16], and $PtAl_2$ [24,25] support SP resonances in this range, which makes an investigation of their plasmonic properties of interest.

$AuAl_2$ films were prepared by e-beam evaporation of a stack of Ti(26 Å)/Au(52 Å)/Al(109 Å)/Au(53 Å)/Al(101 Å) onto the hypotenuse of a right prism made from high refractive index glass (NS-F11). This provides close to a stoichiometric 2:1 ratio of aluminum and gold, with the titanium layer ensuring good adhesion to the glass substrate. After thin film deposition, the prism was immediately annealed at 300 °C for 30 minutes under nearly oxygen- and

water-free conditions in a glove box. This changed the film color to purple, indicating formation of $AuAl_2$. This color does not change appreciably over the course of several months, as $AuAl_2$ is resistant to oxidation in spite of its high aluminum content [26]. Reference films of pure gold were also prepared by evaporating Ti(25 Å) followed by Au(300 Å). These were used without any annealing.

The titanium layers at the bottom of the films are necessary to achieve sufficient adhesion to the glass surface, and even though 25 Å Ti films are almost completely transparent, they are known to introduce additional ohmic losses to the plasmon modes in the nanostructure of which they are part [27,28]. This should have a proportionally smaller effect on the lossier $AuAl_2$ compared to pure gold, and at the relatively low Ti fraction of the film (approx. 8%) that we use here, there should be no appreciable effect on the surface plasmon frequencies of the films [27]. Even the damping effect should be fairly minimal in our case, since the SPs under investigation propagate on the air side of the metal films, with only the evanescent tail of the plasmon mode probing the Ti layer.

As a preliminary characterization of the purple gold films, we measured the visible light spectrum in normal reflection. Two examples are shown in Fig. 1, where the characteristic dip in reflectance centered in the range of 500-550 nm is responsible for the purple color. We used these spectra to calculate CIELAB color coordinates [29] for the reflected light under the assumption of a D65 (average daylight) illuminant, and these are listed in Table 1. Values for the prism used in the experiment are shown along with values measured from both the air and substrate side of a $AuAl_2$ film fabricated on a standard microscope glass slide. Literature values are also shown for reference. The lightness L* varies significantly between samples due to varying degrees of scattering from surface roughness or the degree of transmission through thin films, but the chromatic components (a* and b*) nearly all cluster within relatively narrow ranges, largely as provided by Supansomboon et al. [18], corresponding to colors perceived as purple by most. The biggest outliers here may be the samples characterized by Keast et al. [16,24], which are nearly 15 units bluer on the blue-yellow (b*) axis than the other samples. This may be because these samples were deliberately fabricated with an excess of Al to reduce sample brittleness [16].

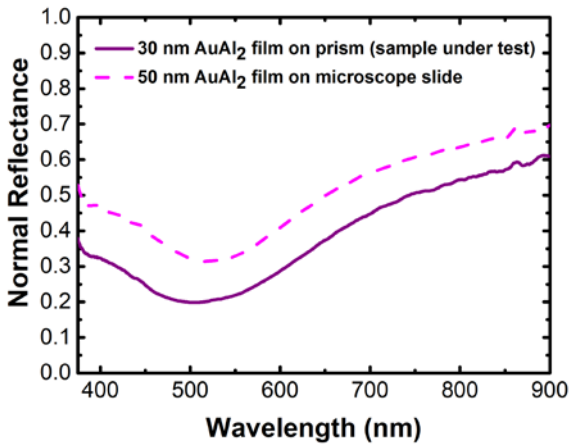

Fig. 1 Normal reflection spectra from 50 nm and 30 nm thick $AuAl_2$ films fabricated as outlined in the text. The dips centered in the 500-550 nm range is responsible for the films' purple color

Table 1 CIELAB colors of different $AuAl_2$ samples. The first line is data from the sample characterized in this paper

Sample/source	Form	L*	a*	b*	Ref.
Film on prism hypothenuse	30 nm film	56.21	14.38	-0.32	
Film on glass slide (top)	50 nm film	66.37	13.78	-4.20	
Film on glass slide (substrate)	50 nm film	55.36	8.80	-5.46	
Cretu & van der Linden (1999)	Bulk	41.3	15.5	-5.0	[3]
Supansomboon et al. (2008)	Films	43 to 65	6.8 to 15.6	-2.2 to -6.1	[18]
Supansomboon et al. (2015)	co-deposit	68.39	17.79	-4.42	[25]
	Stack	65.2	23.38	-9.2	[25]
	Bulk	70.18	10.0	-6.02	[25]
Keast et al. (2011)	Bulk	64.4	14.5	-16.7	[16]
Keast et al. (2013)	Bulk	61.5	18.3	-19.1	[24]

SPs were launched into the film in the Kretschmann configuration [30], where total internal reflection of p-polarized light inside the prism excites the SPs, as shown in Fig. 2. SPs are launched when the wave vector of the reflected wave along the metal-glass interface matches a SP mode travelling along the outer surface of the film, causing a drop in film reflectance. Illuminating with white light, we obtain reflectance spectra as in Fig. 3, where the minima (at λ_{min}) correspond to phase matching with a SP, given by:

$$k_{sp} = \frac{2\pi}{\lambda_{min}} n_p \sin\theta_i \quad ; \quad E_{sp} = \frac{hc}{\lambda_{min}}. \tag{1}$$

k_{sp} and E_{sp} are respectively the wavevector and energy of the surface plasmon, θ_i is the incident angle inside the prism, and n_p is the prism index of refraction.

Taking such spectra as a function of θ_i, we can construct the SP dispersion relation between the light line in vacuum ($E = \hbar kc$) and in the prism ($E = \hbar kc/n_p$). This works well for gold, where the SP is spectrally relatively narrow. SPs in purple gold are significantly lossier, which leads to broad and shallow minima in the reflectance spectrum. Such minima can be difficult to distinguish accurately, so we increase the visibility of the SP through a phase-polarization contrast measurement [31]. This technique takes advantage of the rapid phase change that reflected p-polarized light undergoes when either θ_i or E are tuned through the SP. Since s-polarized light undergoes no such phase change, we can determine the conditions for SP excitation by reflecting both s- and p-polarized light off the film with an intensity ratio and relative phase shift determined respectively by a polarizer (P1 in Fig. 2) and a $\lambda/4$ plate, and then interfering the reflected components in a second polarizer (P2) set at 45° to the polarization axes. This ensures a strong minimum in the reflected light even with lossy surface plasmons. This can be seen in Fig. 3, where we observe distinct minima in reflection spectra from a purple gold film obtained with this technique.

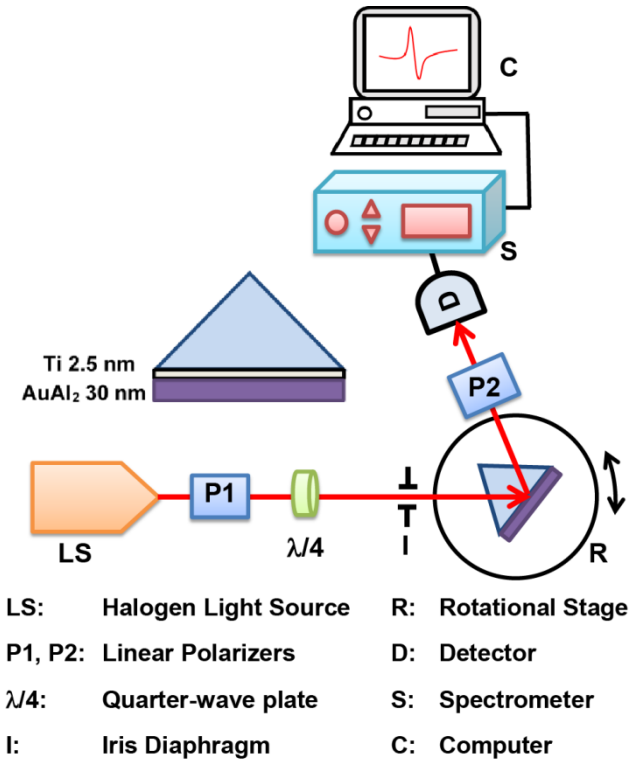

Fig. 2 Setup for launching surface plasmon in thin films based on the Kretschmann configuration. The setup implements a phase-polarization contrast technique to improve the plasmon detectability in our $AuAl_2$ films

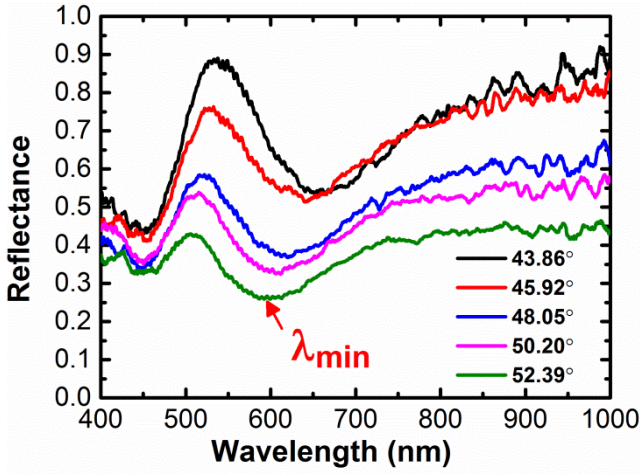

Fig 3 p-polarization reflectance (normalized by s-polarization reflectance) versus wavelength in a thin film of $AuAl_2$ collected with the setup shown in Fig. 2. Each curve corresponds to a different incident angle $\boldsymbol{\theta_i}$ and has its own λ_{min} from which the surface plasmon dispersion relation can be found

With this method, we measured the SP dispersion for 30 nm thick films of $AuAl_2$ and pure gold. These are plotted in Fig. 4 along with theoretical predictions based on literature values for the dielectric functions of gold [17] and purple gold [18]. The location of the SP is given by

$$k_{sp} = \frac{E_{sp}}{\hbar c}\sqrt{\frac{\varepsilon_d \varepsilon_m}{\varepsilon_d + \varepsilon_m}} \tag{2}$$

where ε_m and ε_d are respectively the dielectric functions for the metal film and the medium in contact with the film. In this case, the prism is located in air, so $\varepsilon_d = 1$.

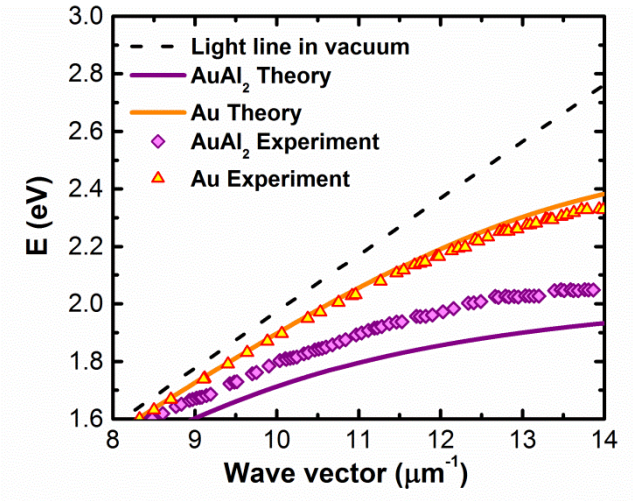

Fig. 4 Calculated (purple line) and measured (purple diamonds) SP dispersion relations of $AuAl_2$ film. The dash-dotted black line is the light line in vacuum $\boldsymbol{\omega = c_0 k}$. The orange curves are for a Au film, shown for comparison and confirming that our experimental result agree well with theory

For both Au and $AuAl_2$, the measured dispersions show the expected bending below the vacuum light line, approaching a constant energy $\hbar\omega_{sp}$ at large wave vectors. Experiment and theory agree well for the pure gold film, but somewhat less well for $AuAl_2$. This may be due to inaccuracies in the published dielectric function for purple gold, or to our film deviating from perfect stoichiometry. In fact, the b* color coordinate indicates that the film being tested here is somewhat more yellow (b*=-0.32) than other films reported in the literature, pointing to a possible excess of Au in the film. Looking at Fig. 1, we discover that this color difference can be attributed to a 20-30 nm (or about 0.1 eV) blue shift in the dip in the reflectance curve obtained from the film used to produce the data in Fig 4 (fabricated on a prism hypothenuse) relative to the film fabricated on a microscope slide. The latter sample is in turn close in color to the samples used to deduce the index of refraction underlying the theoretical curve [18]. Our experimental results yield a value of $\hbar\omega_{sp}^{AuAl_2} = 2.1$ eV, while the theoretical curve indicates $\hbar\omega_{sp}^{AuAl_2} = 1.9$ eV. This difference is consistent with the color shifts just noted, and should be compared to $\hbar\omega_{sp}^{Au} = 2.5$ eV for gold [32].

To further explore the potential of $AuAl_2$ as a plasmonic material, we next demonstrate that it can be used in SPR sensing [33], although we hasten to note that it is not likely to be a good replacement for gold in this particular application, due to its greater optical losses. SPR sensing is based on the dependence, evident in Eq. 2, of the SP dispersion on ε_d. Since the SP decays exponentially above the film, it is only sensitive to changes within a few hundred nm of the film, and can therefore be used to measure adsorption of thin films on the substrate.

Because of the low SP energy in $AuAl_2$, we used a 785 nm wavelength laser for this measurement. We also reverted to detecting only the p-polarization reflectance rather than using phase-polarization contrast measurements. The prism was mounted onto a flow cell, so that we could vary the refractive index near the film. We fixed θ_i to 53.2° since the reflectance curve in water (see Fig. 5) has the highest slope at this wavelength, yielding the highest sensitivity to changes in $n = \sqrt{\varepsilon_d}$.

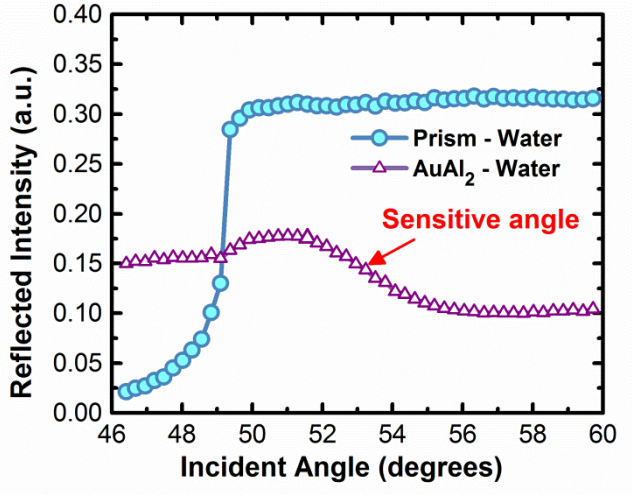

Fig. 5 Plots of measured reflectance curves for p-polarized light incident from the substrate onto a $AuAl_2$ film immersed in water (purple triangles) and onto the substrate-water interface without a metal film present (blue circles). The abrupt onset of high reflectance near 49° in the latter curve marks the onset of total internal reflection. Measurements were performed at $\boldsymbol{\theta_i} = 53.2°$, indicated as the "sensitive angle"

Solutions of sucrose in DI water were used to create well-defined changes in the index of refraction [34]. Fig. 6 shows changes in reflected intensity as water and sucrose solutions of varying concentrations are alternately injected into the flow cell. Index changes of the order of one part in 10^4 are readily detectable. Table 2 summarizes the different preparations along with resulting changes in reflectance, which are linear in the change in refractive index Δn. For this film, the signal change is about 0.95‰ for $\Delta n = 10^{-4}$. This is a rather low sensitivity, but nonetheless confirms the unusually low-lying surface plasmon in $AuAl_2$.

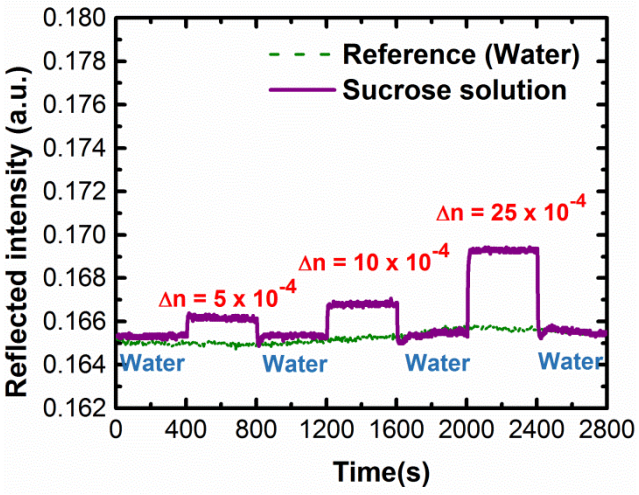

Fig. 6 SPR signal from a 30 nm thick $AuAl_2$ film where water and sucrose solutions were alternately injected to vary the index of refraction

Table 2 Sucrose solutions used for the SPR sensing study

Solutions (at 20°C)	n[a]	Δn vs water	%ΔSignal ($AuAl_2$)
DI Water (reference)	1.3330	0	-
0.35% w/w sucrose	1.3335	5×10^{-4}	0.47
0.70% w/w sucrose	1.3340	10×10^{-4}	0.95
1.75% w/w sucrose	1.3355	25×10^{-4}	2.43

[a] As per Official Method 990.35A of AOAC International

In practical plasmonic applications, $AuAl_2$ will most likely be used in nanoparticle form. Such particles have not yet been made, but we can nonetheless estimate their optical properties from the bulk dielectric function [18], the validity of which we have just verified. Fig. 7 displays the theoretical scattering and absorption cross sections for spherical 20 nm diameter nanoparticles made from either $AuAl_2$ or pure gold, which is shown for comparison.

The broad plasmon peak in $AuAl_2$ nanoparticles results in very strong light absorption throughout the ultraviolet and visible spectrum. The calculations predict that a 20 nm diameter $AuAl_2$ nanoparticle will have a nearly uniform light absorption cross section from 300 nm to 750 nm of about 3×10^{-4} μm^2, or approximately 1.3×10^{-17} cm^2/atom. This is about an order of magnitude greater than in light-absorbing black carbon [35], and comparable to the peak absorbance in single-walled carbon nanotubes [36].

This makes these particles interesting as nanoscale light absorbers in applications where high absorbance in a small volume is of critical importance so that the use of gold can be justified. Examples of such applications may include obscurants [37], ultrathin absorptive neutral density light filters, solar steam generation [38], and photothermal cancer therapy [39-42]. For the latter application, we note that the particles would have significant absorption beyond 650 nm, within the so called biological window of transparency [43], even though they are simple spheres. This distinguishes purple gold from other metals, where more complex

particle structures such as shells or rods are required to achieve surface plasmon resonances in the infrared [39-42].

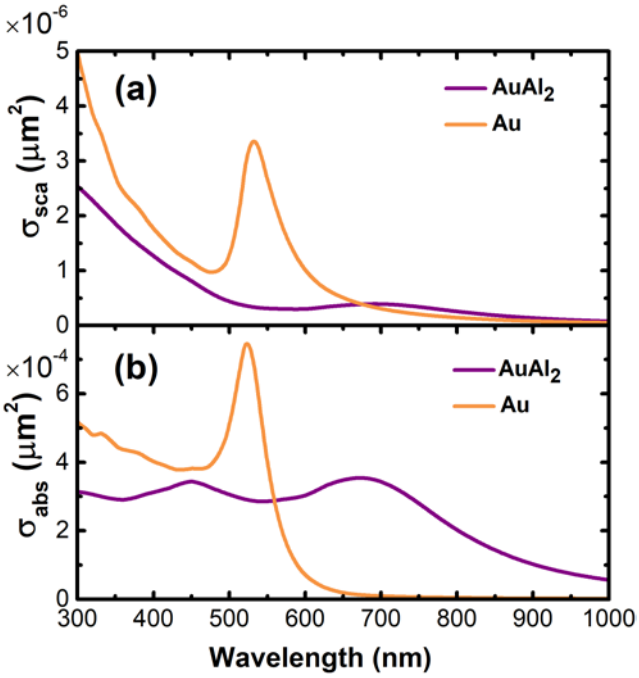

Fig. 7 (a) Calculated scattering cross section and **(b)** absorption cross section spectra of 20 nm diameter $AuAl_2$ (purple lines) and Au (yellow lines) nanospheres in water suspension

The broad absorptivity of $AuAl_2$ nanoparticles may also make them of interest for plasmonic catalysis [44-48], a burgeoning field where the decay of plasmons into hot carriers is used effectuate chemical reactions on the particles' surfaces. In plasmonic catalysis, dampening of plasmons, which predominantly occurs through the excitation of hot carriers, drives the catalysis [44,45]. The lossiness of plasmons in $AuAl_2$ may therefore help rather than hinder catalytic processes. In this context it is worth noting that gold-mediated photocatalytic processes are also observed in gold clusters too small to exhibit plasmon resonances, ranging from cluster sizes of a few dozen gold nuclei [49] all the way down to di- and mononuclear gold clusters [50]. However, in these cases, the photocatalytic activity most likely originates from the excitation of single carriers to discrete excited states and bands rather than on collective excitations such as plasmons.

The cross sections in Fig. 7 are based on bulk measurements, and resonances in single-crystal particles may well be stronger, as surface plasmon resonance quality is often higher in single crystal particles than in polycrystalline ones [51]. In fact, Keast et al. has published a calculation predicting that the plasmon resonance in $AuAl_2$ particles should be comparable in strength to Au particles, significantly stronger than what is shown in Fig. 7 [24]. The discrepancy between theory and bulk measurements was explained by invoking defects in polycrystalline purple gold that would generate increased electron scattering and therefore plasmon losses. This is supported by the drab appearance of as-cast $AuAl_2$ films, the purple color gradually deepening as crystal size increases under annealing. Experiments also show

that the color of $AuAl_2$ can be destroyed by ion irradiation and then restored by annealing [52].

It would therefore be of significant interest to study the plasmonic properties of single crystal $AuAl_2$ nanoparticles to determine if their plasmon resonances are of higher quality than bulk measurements indicate. This, along with the long wavelength of their plasmon resonance, may make them interesting for applications such as metal-enhanced fluorescence [53-57].

In summary, we have launched surface plasmons in thin films of the intermetallic $AuAl_2$, also known as purple gold. The surface plasmon dispersion relation was measured, and is consistent with a surface plasmon energy of $\hbar\omega_{sp}$= 2.10 eV, unusually low for a metal. Although the SPs in this material are lossier than in pure gold, they are still of sufficient quality that they can be used in SPR sensors with reasonable sensitivity. From an applications perspective, $AuAl_2$ is probably of the greatest interest in nanoparticle form, where solid spherical particles would exhibit strong absorption from the ultraviolet into the near infrared, giving it potential applications in areas such as photothermal therapy, solar steam generation, or plasmonic redox catalysis.

We gratefully acknowledge funding from the Institute for Critical Technology and Applied Science (ICTAS) at Virginia Tech.

References

1. Harman G (2010) Gold-Aluminum Intermetallic Compounds and Other Metallic Interface Reactions in Wire Bonding. In: Wire Bonding in Microelectronics. 3rd edn. McGraw Hill, pp 131-182
2. Roberts-Austen WC (1891) On the Melting Points of the Gold-Aluminium Series of Alloys. Proc R Soc Lond 50:367-368. doi:10.1098/rspl.1891.0047
3. Cretu C, van der Lingen E (1999) Coloured gold alloys. Gold Bull 32 (4):115-126. doi:10.1007/bf03214796
4. Cahn RW (1998) Materials science: A precious stone that isn't. Nature 396 (6711):523-524. doi:10.1038/25010
5. Klotz U (2010) Metallurgy and processing of coloured gold intermetallics — Part I: Properties and surface processing. Gold Bull 43 (1):4-10. doi:10.1007/bf03214961
6. Philofsky E (1970) Intermetallic formation in gold-aluminum systems. Solid-State Electronics 13 (10):1391-1394. doi:10.1016/0038-1101(70)90172-3
7. Majni G, Nobili C, Ottaviani G, Costato M, Galli E (1981) Gold-aluminum thin-film interactions and compound formation. J Appl Phys 52 (6):4047-4054. doi:10.1063/1.329214
8. Xu C, Sritharan T, Mhaisalkar SG (2007) Interface transformations in thin film aluminum–gold diffusion couples. Thin Solid Films 515 (13):5454-5461. doi:10.1016/j.tsf.2007.01.017
9. Xu H, Liu C, Silberschmidt VV, Pramana SS, White TJ, Chen Z, Sivakumar M, Acoff VL (2010) A micromechanism study of thermosonic gold wire bonding on aluminum pad. J Appl Phys 108 (11):-. doi:10.1063/1.3514005
10. Noolu N, Murdeshwar N, Ely K, Lippold J, Baeslack W (2004) Phase transformations in thermally exposed Au-Al ball bonds. J Electron Mater 33 (4):340-352. doi:DOI 10.1007/s11664-004-0141-7
11. Hüfner S, Wernick JH, West KW (1972) The density of states of AuAl2, AuIn2 and AuGa2. Solid State Commun 10 (11):1013-1016. doi:10.1016/0038-1098(72)90885-X

12. Wernick JH, Menth A, Geballe TH, Hull G, Maita JP (1969) Superconducting, thermal and magnetic susceptibility behavior of some intermetallic compounds with the fluorite structure. J Phys Chem Solids 30 (8):1949-1956. doi:10.1016/0022-3697(69)90171-1
13. Switendick AC, Narath A (1969) Band structure and ^{197}Au Nuclear-Magnetic Resonance Studies in $AuAl_2$, $AuGa_2$, and $AuIn_2$. Phys Rev Lett 22 (26):1423-1426. doi:10.1103/PhysRevLett.22.1423
14. Perez I, Qi B, Liang G, Lu F, Croft M, Wieliczka D (1988) Spectroscopic results on the above and below E_F electronic structure of TAl_2, T=Au and Pt. Phys Rev B 38 (17):12233-12237. doi:10.1103/PhysRevB.38.12233
15. Hsu L-S, Guo GY, Denlinger JD, Allen JW (2001) Experimental and theoretical study of the electronic structure of AuAl2. J Phys Chem Solids 62 (6):1047-1054. doi:10.1016/S0022-3697(00)00275-4
16. Keast VJ, Birt K, Koch CT, Supansomboon S, Cortie MB (2011) The role of plasmons and interband transitions in the color of AuAl2, AuIn2, and AuGa2. Appl Phys Lett 99 (11):-. doi:10.1063/1.3638061
17. Johnson PB, Christy RW (1972) Optical Constants of the Noble Metals. Phys Rev B 6 (12):4370-4379. doi:10.1103/PhysRevB.6.4370
18. Supansomboon S, Maaroof A, Cortie MB (2008) "Purple glory": The optical properties and technology of AuAl2 coatings. Gold Bull 41 (4):296-304. doi:10.1007/bf03214887
19. Maier SA (2007) Plasmonics: Fundamentals and Applications. Springer. doi:10.1007/0-387-37825-1
20. Ozbay E (2006) Plasmonics: Merging Photonics and Electronics at Nanoscale Dimensions. Science 311 (5758):189-193. doi:10.1126/science.1114849
21. Pelton M, Aizpurua J, Bryant G (2008) Metal-nanoparticle plasmonics. Laser Photonics Rev 2 (3):136-159. doi:10.1002/lpor.200810003
22. Brolo AG (2012) Plasmonics for future biosensors. Nat Photon 6 (11):709-713. doi:10.1038/nphoton.2012.266
23. Naik GV, Shalaev VM, Boltasseva A (2013) Alternative Plasmonic Materials: Beyond Gold and Silver. Adv Mater 25 (24):3264-3294. doi:10.1002/adma.201205076
24. Keast VJ, Zwan B, Supansomboon S, Cortie MB, Persson POÅ (2013) AuAl2 and PtAl2 as potential plasmonic materials. J Alloy Compd 577 (0):581-586. doi:10.1016/j.jallcom.2013.06.161
25. Supansomboon S, Dowd A, Gentle A, van der Lingen E, Cortie MB (2015) Thin films of PtAl2 and AuAl2 by solid-state reactive synthesis. Thin Solid Films 589:805-812. doi:10.1016/j.tsf.2015.07.019
26. Moser M, Mayrhofer PH, Ross IM, Rainforth WM (2007) Thermal stability of sputtered intermetallic Al–Au coatings. J Vac Sci Technol A 25 (5):1402-1406. doi:10.1116/1.2757181
27. Debu DT, Ghosh PK, French D, Herzog JB (2017) Surface plasmon damping effects due to Ti adhesion layer in individual gold nanodisks. Opt Mater Express 7 (1):73-84. doi:10.1364/OME.7.000073
28. Habteyes TG, Dhuey S, Wood E, Gargas D, Cabrini S, Schuck PJ, Alivisatos AP, Leone SR (2012) Metallic Adhesion Layer Induced Plasmon Damping and Molecular Linker as a Nondamping Alternative. ACS Nano 6 (6):5702-5709. doi:10.1021/nn301885u
29. ASTM (2017) Standard Practice for Computing the Colors of Objects by Using the CIE System. E308-17.
30. Kretschmann E, Raether H (1968) Radiative decay of nonradiative surface plasmons excited by light. Z Naturforch A 23:2135-2136. doi:10.1515/zna-1968-1247
31. Kabashin AV, Kochergin VE, Beloglazov AA, Nikitin PI (1998) Phase-polarisation contrast for surface plasmon resonance biosensors. Biosens Bioelectron 13 (12):1263-1269. doi:10.1016/S0956-5663(98)00088-8

32. Rhodes C, Franzen S, Maria JP, Losego M, Leonard DN, Laughlin B, Duscher G, Weibel S (2006) Surface plasmon resonance in conducting metal oxides. J Appl Phys 100 (5). doi:10.1063/1.2222070
33. Homola J (ed) (2006) Surface Plasmon Resonance Based Sensors. Springer Series on Chemical Sensors and Biosensors, vol 4. Springer,
34. Latimer Jr. GW, ed. (ed) (2012) Official Methods of Analysis of AOAC International, Vol. II, vol II. 19th edn. AOAC International,
35. Bond TC, Bergstrom RW (2006) Light Absorption by Carbonaceous Particles: An Investigative Review. Aerosol Sci Technol 40 (1):27-67. doi:10.1080/02786820500421521
36. Streit JK, Bachilo SM, Ghosh S, Lin C-W, Weisman RB (2014) Directly Measured Optical Absorption Cross Sections for Structure-Selected Single-Walled Carbon Nanotubes. Nano Lett 14 (3):1530-1536. doi:10.1021/nl404791y
37. Paul GA (2007) Modelled infrared extinction and attenuation performance of atmospherically disseminated high aspect ratio metal nanoparticles. J Opt A 9 (3):278. doi:10.1088/1464-4258/9/3/012
38. Neumann O, Urban AS, Day J, Lal S, Nordlander P, Halas NJ (2013) Solar Vapor Generation Enabled by Nanoparticles. ACS Nano 7 (1):42-49. doi:10.1021/nn304948h
39. Huang XH, El-Sayed IH, Qian W, El-Sayed MA (2006) Cancer cell imaging and photothermal therapy in the near-infrared region by using gold nanorods. J Am Chem Soc 128 (6):2115-2120. doi:10.1021/Ja057254a
40. Gobin AM, Lee MH, Halas NJ, James WD, Drezek RA, West JL (2007) Near-Infrared Resonant Nanoshells for Combined Optical Imaging and Photothermal Cancer Therapy. Nano Lett 7 (7):1929-1934. doi:10.1021/nl070610y
41. Kennedy LC, Bickford LR, Lewinski NA, Coughlin AJ, Hu Y, Day ES, West JL, Drezek RA (2011) A New Era for Cancer Treatment: Gold-Nanoparticle-Mediated Thermal Therapies. Small 7 (2):169-183. doi:10.1002/smll.201000134
42. Lissett B, Jiantang S, Kun F, Nastassja L, Vengadesan N, Joseph C, Rebekah D (2008) Enhanced multi-spectral imaging of live breast cancer cells using immunotargeted gold nanoshells and two-photon excitation microscopy. Nanotechnol 19 (31):315102. doi:10.1088/0957-4484/19/31/315102
43. Weissleder R (2001) A clearer vision for in vivo imaging. Nat Biotechnol 19 (4):316-317. doi:10.1038/86684
44. Aslam U, Chavez S, Linic S (2017) Controlling energy flow in multimetallic nanostructures for plasmonic catalysis. Nat Nanotech 12:1000. doi:10.1038/nnano.2017.131
45. Zhang X, Li X, Reish ME, Zhang D, Su NQ, Gutiérrez Y, Moreno F, Yang W, Everitt HO, Liu J (2018) Plasmon-Enhanced Catalysis: Distinguishing Thermal and Nonthermal Effects. Nano Lett 18 (3):1714-1723. doi:10.1021/acs.nanolett.7b04776
46. Ren X, Cao E, Lin W, Song Y, Liang W, Wang J (2017) Recent advances in surface plasmon-driven catalytic reactions. RSC Advances 7 (50):31189-31203. doi:10.1039/C7RA05346K
47. Zhang XM, Chen YL, Liu RS, Tsai DP (2013) Plasmonic photocatalysis. Rep Prog Phys 76 (4)
48. Christopher P, Xin H, Marimuthu A, Linic S (2012) Singular characteristics and unique chemical bond activation mechanisms of photocatalytic reactions on plasmonic nanostructures. Nature Mater 11:1044. doi:10.1038/nmat3454
49. Chen H, Liu C, Wang M, Zhang C, Luo N, Wang Y, Abroshan H, Li G, Wang F (2017) Visible Light Gold Nanocluster Photocatalyst: Selective Aerobic Oxidation of Amines to Imines. ACS Catalysis 7 (5):3632-3638. doi:10.1021/acscatal.6b03509
50. Huang L, Rudolph M, Rominger F, Hashmi ASK (2016) Photosensitizer-Free Visible-Light-Mediated Gold-Catalyzed 1,2-Difunctionalization of Alkynes. Angew Chem Int Ed 55 (15):4808-4813. doi:10.1002/anie.201511487

51. Ditlbacher H, Hohenau A, Wagner D, Kreibig U, Rogers M, Hofer F, Aussenegg FR, Krenn JR (2005) Silver Nanowires as Surface Plasmon Resonators. Phys Rev Lett 95 (25):257403. doi:10.1103/PhysRevLett.95.257403
52. Furrer A, Seita M, Spolenak R (2013) The effects of defects in purple AuAl2 thin films. Acta Mater 61 (8):2874-2883. doi:10.1016/j.actamat.2013.01.029
53. Geddes CD, Lakowicz JR (2002) Metal-enhanced fluorescence. J Fluoresc 12 (2):121-129. doi:10.1023/A:1016875709579
54. Tam F, Goodrich GP, Johnson BR, Halas NJ (2007) Plasmonic Enhancement of Molecular Fluorescence. Nano Lett 7 (2):496-501. doi:10.1021/nl062901x
55. Geddes CD (ed) (2010) Metal-Enhanced Fluorescence. John Wiley & sons,
56. Deng W, Xie F, Baltar HTMCM, Goldys EM (2013) Metal-enhanced fluorescence in the life sciences: here, now and beyond. Phys Chem Chem Phys 15 (38):15695-15708. doi:10.1039/c3cp50206f
57. Racknor C, Singh MR, Zhang Y, Birch DJS, Chen Y (2014) Energy transfer between a biological labelling dye and gold nanorods. Methods Appl Fluoresc 2 (1):015002